

# Flows, Fragmentation, and Star Formation. I. Low-mass Stars in Taurus

Lee Hartmann

*Harvard-Smithsonian Center for Astrophysics, 60 Garden St., Cambridge, MA 02138;  
Electronic mail: hartmann@cfa.harvard.edu*

## ABSTRACT

The remarkably filamentary spatial distribution of young stars in the Taurus molecular cloud has significant implications for understanding low-mass star formation in relatively quiescent conditions. The large scale and regular spacing of the filaments suggests that small-scale turbulence is of limited importance, which could be consistent with driving on large scales by flows which produced the cloud. The small spatial dispersion of stars from gaseous filaments indicates that the low-mass stars are generally born with small velocity dispersions relative to their natal gas, of order the sound speed or less. The spatial distribution of the stars exhibits a mean separation of about 0.25 pc, comparable to the estimated Jeans length in the densest gaseous filaments, and is consistent with roughly uniform density along the filaments. The efficiency of star formation in filaments is much higher than elsewhere, with an associated higher frequency of protostars and accreting T Tauri stars. The protostellar cores generally are aligned with the filaments, suggesting that they are produced by gravitational fragmentation, resulting in initially quasi-prolate cores. Given the absence of massive stars which could strongly dominate cloud dynamics, Taurus provides important tests of theories of dispersed low-mass star formation and numerical simulations of molecular cloud structure and evolution.

*Subject headings:* stars: formation, pre-main sequence

## 1. Introduction

The Taurus-Auriga molecular cloud long has been a touchstone for studies of star formation. Although Taurus is not typical of most (massive) star-forming regions, its proximity and low extinction mean that its stellar population is the best determined of any star-forming cloud. Perhaps more importantly, Taurus is relatively quiescent, with low turbulent velocities and a lack of massive stars to dissociate, ionize, and otherwise disrupt the cloud. If the simple, static models of the original paradigm of low-mass star formation (e.g., Shu, Adams, & Lizano 1987) can be applied anywhere, they should work in Taurus.

The spatial distributions with which stars are formed can provide important clues to the processes of star formation. Even though Taurus does not contain populous clusters, many of its stars

fall into loose groups (Jones & Herbig 1979; Gomez et al. 1993). So far, the most detailed studies of the stellar spatial distribution in Taurus have considered the two-point correlation function (Gomez et al. 1993) and the related mean surface density of companions (MSDC; Larson 1995). Larson (1995) found that the MSDC exhibited roughly two distinct power-law distributions at small and large scales, the inner region corresponding to close binaries and multiple systems, and the outer region representing the clustering properties of the stars. A break between these two distributions was identified at about  $\sim 0.04$  pc, which Larson suggested was the Jeans length in Taurus (see also Simon 1997 and Bate, Clarke, & McCaughrean 1998).

The molecular gas in Taurus has long been recognized to be filamentary in nature (e.g., Schneider & Elmegreen 1979; Scalo 1990; Mizuno et al. 1995). It is also well-recognized that the young stars are strongly correlated with gas and dust; i.e., that the stellar distribution must exhibit filamentary structure as well. However, the extent of the stellar filamentary distribution, and its physical significance, has not been given sufficient attention, nor has it been viewed in the context of recent numerical simulations of molecular clouds. The spatial distribution of young objects in Taurus is reexamined from this point of view, with emphasis on its relationship to our previous suggestion that the Taurus cloud (like other nearby molecular clouds) was formed by large-scale flows in the interstellar medium (Ballesteros-Paredes, Hartmann, & Vazquez-Semadeni 1999, BHV; Hartmann, Ballesteros-Paredes, & Bergin 2001, HBB).

## 2. Spatial distribution

### 2.1. Sample

The basic sample of young stars in Taurus used in this paper is taken from the tabulation of Kenyon & Hartmann (1995) with various additions. A few new low-mass stars were added from the studies of Briceño et al. (1998, 1999). I further added a few stars from the Rosat All-Sky Survey (RASS) studies of Wichmann et al. (1996, 2000).

Some investigators have argued that the RASS identified large numbers of previously unknown, much older Taurus members (e.g., Neuhäuser et al. 1995; Wichmann et al. 1996), a claim that does not hold up under detailed scrutiny (Briceño et al. 1997; Martin & Magazzu 1998; HBB). However, for present purposes any possible older population is unimportant, because these stars can and probably have dispersed significantly from their birthsites, and so their positions reveal little about star formation processes. For this reason neither the “post-T Tauri” stars identified on the basis of Li by Martin & Magazzu (1998) nor the “zero age main sequence” stars of Wichmann et al. (2000) have been included. I have also eliminated a number of stars originally in Kenyon & Hartmann (1995) which were taken from the study of Walter et al. (1988), based on low Li abundances and also positions in the HR diagram indicating ages greatly in excess of 10 Myr. Note that if all potential pre-main sequence X-ray members were added to the sample, there would be little effect on the subsequent conclusions, because these stars are widely dispersed spatially, and thus constitute a

small fraction of the objects in the area under consideration.

## 2.2. Group structure

Figure 1 shows the spatial distribution of young stellar objects superimposed upon the  $^{12}\text{CO}$  map of Megeath, Dame, & Thaddeus (2002). Apart from a few small, localized, widely distributed groups (the largest of which is the L1551 group), most of the Taurus stars are found in three nearly parallel, elongated bands. Even the two groups or mini-clusters of L1495 lie at the western end of the main band. The stellar bands lie along parallel filaments in the molecular gas, recognized earlier from extinction studies (Schneider & Elmegreen 1979). (In the following I use the term “band” to refer to extended distributions of stars, and use “filament” to refer to the narrower dense gas structures and stars near these densest structures.)

Figure 2a shows the spatial distributions of the young stars in the central Taurus region, along with the positions of optically-determined cloud cores from the unbiased survey of Lee & Myers (1999). The overall regularity of the structure is perhaps clearer than in the  $^{12}\text{CO}$  gas. Three main bands of stars appear to be roughly parallel and approximately spaced apart by a projected distance of about 1.5 degrees,  $\sim 3.7$  pc at the 140 pc distance of Taurus (Kenyon, Dobryzcka, & Hartmann 1994). The two groups of the L1495 region are separated from the main stellar band by a similar distance.

Figure 2b shows the distributions of objects sorted into groups somewhat arbitrarily for further analysis; for example, groups 1 and 2 might be merged into one group. Comparison with Figure 2a shows that only a few, widely-dispersed objects have been deleted from the sample. Stars near the two dense groupings in L1495 have also been marked. The members of the groups shown in Figure 2b are listed in Table 1.

Figure 3 shows schematically the approximate positions of the  $^{13}\text{CO}$  filaments identified by Mizuno et al. (1995) superimposed upon the stellar distribution. The positions of the main groups are correlated with the main clusters of gaseous filaments. There is clearly significant substructure within the main bands, especially in the regions of Group 1 and L1495, while Groups 3 and 4 show significantly simpler and much more linear filamentary structure, consistent with the spatial distribution of the stars, as discussed further in §2.3.

The  $^{13}\text{CO}$  data demonstrate a velocity difference between Groups 1 and 2 (connecting the clouds B213, L1521, and Heiles Cloud 2), but this difference may simply reflect the large-scale velocity gradient in Taurus. For the same reason the filament extending westward from the Group 3 may be part of the same structure. Several filaments connect the two concentrations of the L1495 cloud at the western end of the complex, suggesting that these concentrations should be considered together.

Figure 4 shows the distribution of Class I and optical cores. These objects are more closely

correlated in space than the Class II and Class III sources. In particular, the Group 3 objects centered near (l,b = 174, -16) display a remarkably linear structure (associated with the B18 cloud). This structure is considered in more detail in the following section. A section of Group 1 near (l,b = 171, -16) is associated with the narrow B213 filament, and also displays a remarkably narrow structure.

### 2.3. Ages and spatial dispersion

It would not be surprising if the members of these spatially-concentrated groups are in general younger than the rest of the Taurus population. One simple, likely indicator of age is the spectral energy distribution class. One would expect that the Class 0 - I objects (protostars, with remnant infalling envelopes) are in general younger than the (mostly) optically-visible T Tauri stars. In turn, since accretion disks dissipate over time, one would expect the Class III objects (stars without accreting disks) to be older than the Class II objects (T Tauri stars with disk accretion onto the central star). However, there are many Class III objects in Taurus with ages similar to those of Class II stars (Kenyon & Hartmann 1995), showing that the Class II/Class III dichotomy is not merely a function of age. Here the classes listed in Kenyon & Hartmann (1995) have been used when available; otherwise, the 10 Å criterion for the H $\alpha$  equivalent width has been used to distinguish Classical T Tauri stars (II) from Weak T Tauri stars (III).

Of the 204 objects in the total Taurus sample, the numbers of Class I/II/III objects are 24/108/72. The same numbers for groups 1-4 are 19/51/18.<sup>1</sup> (Here the two class I/II objects in the samples, HK Tau and Haro 6-13, have been divided into one net Class I and one net Class II for counting purposes.) L1495 by itself has only one class I object; the ratios are 1/26/13. The total numbers divided by class for the four groups plus L1495 are 20/77/31; therefore, the numbers are 4/31/41 for the Taurus objects outside of the groups and L1495. There is an unsurprising excess of Class I objects in the groups, since the groups are strongly correlated with the dense gas where protostars form. The results also indicate a significant excess of Class III sources in the more distributed population, which would suggest a significant dispersal of accretion disks over a timescale comparable to the median age of Taurus,  $\sim 2$  Myr (Palla & Stahler 2000).

A more direct test of age differences is to plot an HR diagram for the T Tauri stars. Figure 5 shows the results for objects for which spectral types and stellar luminosities are available from either Kenyon & Hartmann (1995) or Briceño et al. (1998). There is some suggestion that the non-grouped stars are older, although much of the effect may be due to inclusion of the L1551

---

<sup>1</sup>The assignment of Class I stars was taken from Kenyon & Hartmann (1995). The compilation of Chen et al. (1995) lists 26 total Class 0 and I Taurus stars, not counting the class 0 source IRAM 04191+1522 found by André, Motte, & Bacmann (1999). The assignment of Class I stars in the groups agrees with that of Chen et al. (1995) except for L1527 = 04368+2557, which Chen et al. identify as a Class 0 source. These small discrepancies in classification are not important for the overall discussion.

group, which previously has been found to exhibit a wide age spread (Gomez et al. 1992). To examine the possible difference in ages in the least model-dependent way, I consider the luminosity distributions of group and non-group stars over a modest range of effective temperature; the luminosity distribution then corresponds to an age distribution (e.g., Hartmann 2001). A two-sided Kolmogorov-Smirnov test of the luminosity distributions of K7-M1 stars indicates no strongly significant difference between the group and non-grouped stars, and thus does not support a significant difference in age for this mass range. Any possible age difference between the group and non-group T Tauri stars needs to be investigated further, with more complete estimates of stellar luminosities and effective temperatures, along with additional examination of possible systematic errors (Hartmann 2001).

The presence of such well-defined bands and filaments in the stellar spatial distribution implies that the stars in the groups must be relatively young and that the internal velocity dispersions must not be very large. One can take advantage of the remarkably linear structure of Group 3 to investigate this in a simple way. A least-squares linear fit to the positions of the Class I objects and cores in galactic coordinates, first removing the one core that deviates strongly (B18-2; Lee & Myers 1999), yields the dotted line shown in Figure 4. The rms dispersion in distance of these 19 objects (13 cores and 6 Class I or I/II objects) from the line is 0.0667 degree, or  $\sim 0.16$  pc. This is remarkably small considering the total length of the distribution is  $\sim 3.93$  degree  $\sim 9.6$  pc. The spatial dispersion of the 17 Class II and Class III objects from the same line is somewhat larger,  $\sim 0.148$  degree  $\sim 0.37$  pc; the dispersion of Class II objects alone is only marginally smaller,  $\sim 0.31$  pc. It should be noted that this difference in spatial dispersion between the Class I/cores and the II/III objects is marginally significant, only about 2.3 standard deviations.

Assuming that the difference in spatial dispersion between the Class I objects and cores on the one hand, and the T Tauri stars on the other, is real and is due entirely to dispersal and not to a difference in birth sites, then an upper limit to the velocity dispersion can be estimated. Assuming the average age of the Taurus stars of  $\sim 2$  Myr (Palla & Stahler 2000; see Hartmann 2001 for the difficulty in assigning individual ages to young stars), this would imply that the Class II/Class III objects of group 3 have a velocity dispersion perpendicular to the filament (in the plane of the sky)  $\lesssim 0.2 \text{ km s}^{-1}$ , comparable to the sound speed at 10 K. If these stars are systematically younger than average (see above), the upper limit to the dispersion might be somewhat larger; on the other hand, the true birthsites of these objects could be more widely spread than the Class I/core objects. In any event, the implied small velocity dispersion emphasizes the quiescent nature of this filament.

#### 2.4. Surface density analysis

As mentioned in the Introduction, the spatial structure of the Taurus YSOs has previously been discussed in terms of companions per unit area, either with the MSDC (Larson 1995; Simon 1997) or the two-point correlation function (Gomez et al. 1993). On large scales, Larson (1995) estimated that the MSDC was approximately a power-law,  $\propto \theta^{-0.62}$ , and suggested that this indicated

hierarchical clustering, perhaps of a fractal nature. The slope of the MSDC changed dramatically at small scales  $\lesssim 0.02$  degree  $\sim 0.05$  pc, at which point binary and multiple systems dominate the rapid rise in the MSDC. Larson interpreted this break as setting the Jeans length in Taurus.

Figure 6 shows an updated version of the MSDC, including additional members of Taurus not known earlier. As discussed in Simon (1997), it is difficult to estimate errors for the MSDC or correlation function because the data bins are not independent. The errors in Figure 6 have been crudely estimated by dividing the Taurus stars into four samples and calculating the resulting dispersion (averaged slightly among bins). Here I concentrate on the structure of the MSDC outside of the “binary” or companion star regime,  $\log \theta \geq -2$ ; the innermost region has been treated in detail by Simon (1997).

Using smaller spatial bins spanning a larger range of separations than considered by Larson (1995) or Simon (1997), the MSDC exhibits an apparently significant break near  $\log \theta = -1$ , which is only hinted at in the results of Simon (1997) but appears more clearly in the results of Gomez et al. (1993) (see their Figure 2). The large-scale MSDC slope is steeper,  $\sim -0.98 \pm 0.04$ , than found by Larson or Simon. The difference appears to be that the previous investigators binned over larger size scales, and limited the fit to smaller scales, so that their fits spanned the turnover at  $\log \theta = -1$ .

The MSDC,  $\Sigma(\theta) \propto \theta^s$ , is the number of companions per unit area, which depends not only upon the tendency of stars to group together, but also the overall geometry of the star-forming region. Consider a simple model in which stars are distributed roughly uniformly along an (infinitely long) filament. On scales larger than the filament width, the number of companions to any given star will increase linearly with increasing distance, while the (two-dimensional) area increases as the square of the distance; thus, the slope of the MSDC should approach  $s \sim -1$ . On scales smaller than the filament width, if the stars are uniformly distributed in space, the MSDC will be flat,  $s \sim 0$ . If the stars within the filament tend to be more clustered,  $s$  will be negative, while if there is a tendency for the stars to be no closer than a certain distance,  $s$  can be positive.

I thus suggest that the filamentary structure in Taurus is mostly responsible for the slope  $s \sim -1$  at large separations, and that the stellar distribution does not exhibit a fractal structure (see Blitz & Williams 1997 for a similar conclusion concerning fractal structure in the gas). There may be problems with this interpretation on the largest scales, because some of the filaments are only a few degrees long; on the other hand, eliminating all the bins with  $\theta > 1$  degree would still yield a similar slope at the largest scales considered. The break between the large-scale structure and the binary distribution at approximately 0.25 pc probably indicates the typical filament width, or some average spacing between stars, or both (§3.3).

### 3. Discussion

#### 3.1. Filaments and turbulence

One of the major problems in molecular cloud formation and evolution is the nature and source(s) of turbulent motions in clouds. Turbulence clearly plays a role in the dynamics of molecular clouds (e.g., Larson 1981); however, recent numerical simulations show that MHD turbulent motions decay rapidly in molecular clouds, generally on a crossing time or free-fall time (Stone, Ostriker, & Gammie 1998; Mac Low et al. 1998; Padoan & Nordlund 1999; Mac Low 1999). If clouds last for a “long time”, this rapid damping of MHD turbulence requires the continual injection of turbulent energy to “support” the cloud against its self-gravity. On the other hand, if clouds do not have long lifetimes (BHV; HBB; Elmegreen 2000), then turbulence need not be regenerated (BHV; Elmegreen 2000; HBB; Pringle, Allen, & Lubow 2001). Locally-generated, stellar-driven turbulence must be important in many regions, especially those in which high-mass stars are formed. Taurus would seem to be a good candidate for minimal effects of local turbulence because it lacks high-mass stars, though low-mass stars may inject substantial amounts of energy through their bipolar outflows (Matzner & McKee 1999, 2000).

Although the general filamentary structure of gas and stars in Taurus has been recognized for some time, its extent is remarkable; the main band (groups 1 and 2) extends essentially from one end of the complex to the other. Furthermore, the other bands are roughly parallel to the main structure. This large-scale organization of the Taurus clouds strongly suggests that any turbulence present must be dominated by a large-scale component, or alternatively, not driven mostly on small scales, a conclusion reinforced by recent numerical simulations of molecular clouds. Many simulations often adopt an *ad hoc* driving force or velocity field, or an initial spectrum of density fluctuations, with a fixed distribution of amplitudes and spatial wavenumbers (e.g., Heitsch, MacLow, & Klessen 2001; Ostriker, Stone, & Gammie 2001; Klessen & Burkert 2000). Consider specifically the simulations of Klessen & Burkert (2000, 2001) and Klessen (2001), who studied the dynamical evolution of an isothermal molecular cloud in a cubical volume, with various assumptions about initial density fluctuations and driving of turbulence on a variety of scales. Unsurprisingly, in the Klessen & Burkert (2000, 2001) simulations with density fluctuations leading to velocity perturbations, or in the Klessen (2001) simulations with energy driving, calculations with significant power in small spatial wavenumbers (on small spatial scales) lead to small-scale structure, while simulations with driving at low wavenumbers (large spatial scales) lead to larger-scale structure, in particular the formation of filaments with large spatial extent relative to the size of the computational volume (for example, Figure 1 of Klessen 2001).

Based on these simulations, as well as simple considerations, it seems unlikely that local turbulent energy injection has produced the bands and filaments of Taurus. Rather, I conjecture that the Taurus cloud structure is consistent with large-scale driving of turbulence. If, as BHV and HBB suggested, large-scale flows are responsible for the formation of the Taurus molecular cloud, such large-scale driving could produce large-scale turbulence and complex-wide structure. These

conclusions are in agreement with the suggestion of Burkert & Mac Low (2002) that such large-scale driving is dominant in many molecular clouds. This is also consistent with observations of low-density, non-self-gravitating molecular clouds, in which structure is observed (sometimes filamentary) that must be driven by external flows (Falgarone et al. 1998; LaRosa, Shore, & Magnani 1999; Sakamoto 2002).

The large-scale magnetic field in the Taurus region is well-ordered, and oriented roughly perpendicular (in projection) to the filaments (Moneti et al. 1984; Heyer et al. 1987). This is also consistent with large-scale, ordered turbulence, as simulations with comparable magnetic and flow energies show that the turbulent motions carry the field around as much as the field channels the flow (see discussion in HBB). In this way the magnetic field may provide a preferential direction for concentration.

In general, one might expect that colliding flows tend to produce more sheet-like distributions than filaments, although both are possible results of turbulence (e.g., Klein & Woods 1998). One way of producing filaments from sheets, suggested by Schneider & Elmegreen (1979), and pointed out to the author by P. Myers (personal communication), is by gravitational fragmentation (e.g., Miyama et al. 1987a,b; Nakajima & Hanawa 1996). Using the extreme limiting case of an isothermal, static, self-gravitating sheet, the critical wavelength is  $\sim 2\pi H$ , where  $H$  is the scale height (Larson 1985). The  $\sim 3.7$  pc separation of the filaments would then suggest a full thickness of the initial sheet of only  $\sim 1$  pc. The sheet thickness could be even less if one assumes that the filaments are produced by the fastest growing modes, not the critical one (e.g., Miyama et al. 19897a,b; Nakajima & Hanawa 1996). As the Taurus molecular gas is not static but contains supersonic turbulence, and as it is highly unlikely to be in hydrostatic equilibrium, these estimates is highly uncertain. Nevertheless, if the thickness of the sheet or individual filaments were much greater than 1 pc, they would have to be oriented almost precisely along the line of sight. This seems unlikely, particularly for the Group 3 structure; an intrinsically filamentary structure seems more probable (e.g., Schneider & Elmegreen 1979).

In addition, if the clouds are produced by oblique flows, the resulting turbulent velocity dispersion in the post-shock flow might well be anisotropic, providing a preferential direction for gravitational contraction. Numerical simulations are needed to test this possibility for enhancing formation of filaments.

### 3.2. Filaments and fragmentation

Broadly speaking, there are two extreme views of how protostellar cores are fragmented from their surrounding molecular cloud. One posits gravitational fragmentation into Jeans-mass-sized objects (e.g., Larson 1985); the other supposes that turbulent flows concentrate mass into cores which then are gravitationally-bound (e.g., Padoan & Nordlund 1999), or that the cloud has a highly complex, hierarchical if not fractal structure (Elmegreen 1997) not primarily driven by



gravity. The true situation must fall somewhere in between these extremes, as star-forming clouds exhibit supersonic turbulence which must be damped to some extent before gravitational collapse can proceed, and any concentrations of gas formed by turbulence will only form stars if they satisfy a Jeans criterion.

Larson (1985) emphasized that gravitational fragmentation generally requires the presence of substructure, such as sheets or filaments, to provide a smaller scale length than the entire cloud. The fragmentation length is generally a small multiple of a characteristic scale length in the gas (e.g., Oganessian 1960a,b; Chandrasekhar & Fermi 1953). In an equilibrium self-gravitating sheet or filament, for example, the scale height is by definition the length scale over which pressure forces can resist gravity; the Jeans length along the sheet or filament then must be a few times larger than the scale height.

The filamentary structure of the stellar distribution in Taurus suggests that gravitational fragmentation in the filaments should be considered as a mechanism for forming cores. The extreme contrary view, in which flows create isolated cores, is difficult to fit in with the observed linear morphology of Taurus; one would expect much more distributed, “frothy” or bubble-shaped structures. It should be acknowledged that some of the stars in Taurus may result from such flows, particularly in the more distributed areas, and perhaps such flows are responsible for formation of tighter groups such as the L1551 region; however, even some of the distributed regions do appear to be elongated, and there is evidence in the  $^{12}\text{CO}$  map for an extended gaseous filament to the west of L1551 (see Figure 1).

Although the Taurus filaments exhibit supersonic motions, it is useful to begin by reviewing the properties of isothermal, infinite, self-gravitating cylinders as a starting point. Consider a cylinder infinitely extended in the  $z$  direction, with  $R$  the radial distance in cylindrical coordinates. The critical line density (mass per unit length in the  $z$  direction) is a function only of temperature (Ostriker 1964);

$$m = 2c_s^2/G, \quad (1)$$

where  $c_s$  is the isothermal sound speed. Assuming a mean molecular weight of  $2.36m_H$ , this line density corresponds to

$$m = 16.3 T_{10} M_\odot \text{ pc}^{-1}, \quad (2)$$

where  $T_{10}$  is the gas temperature in units of 10 K. Line densities above this critical value result in collapse in the  $R$  direction. The Jeans length in the  $z$  dimension for the cylinder of critical line density is (Larson 1985)

$$\lambda_c = 3.94 c_s^2/(G\Sigma_0) \quad (3)$$

or

$$\lambda_c = 1.5 T_{10} A_V^{-1} \text{ pc}. \quad (4)$$

Here  $A_V$  is the visual extinction through the center of the filament, and  $\Sigma$  is the corresponding surface density, where I use the conversion  $A_V = \Sigma/4.4 \times 10^{-3} \text{ g cm}^{-2}$ . The corresponding critical

mass for this fragment is (Larson 1985)

$$M_c = 24 T_{10}^2 A_V^{-1} M_\odot. \quad (5)$$

The filament has a density structure as a function of cylindrical radius  $R$  of

$$\rho = \rho_0 (1 + R^2/(4H^2))^{-2}, \quad (6)$$

where the scale height  $H$  is given by

$$H = c_s^2/(2G\Sigma_0) = 0.19 T_{10} A_V^{-1} \text{ pc}. \quad (7)$$

A fragmenting filament will clearly be elongated in the  $z$  direction, at least initially (Oganessian 1960b; Chandrasekhar & Fermi 1953; Larson 1985). In terms of the diameter of the filament at which the density falls to one-half its central value,  $d(\rho) = 2.57H$ , the aspect ratio is  $\lambda_c/d(\rho) = 3.09$ . In terms of the half-mass diameter  $d(m) = 4H$  (e.g., Ostriker 1964), the aspect ratio is  $\lambda_c/d(m) \sim 2$ . Note that the aspect ratio is independent of temperature and density.

It is also of interest to consider the linear growth time for gravitational instability. Larson (1985) extrapolated the results from the incompressible filament to estimate a rough linear growth rate for the isothermal cylinder. From Larson’s Figure 1 the growth timescale is estimated to be

$$\tau \sim 3.7 T_{10}^{1/2} A_V^{-1} \text{ Myr}. \quad (8)$$

Now compare this limiting static model with the real Taurus filaments and bands. Table 2 lists lengths and number densities of stars in the several groups. For the purpose of determining line number densities for the main regions of the groups, the westernmost member of group 3 and the easternmost one and two members of groups 2 and 4, respectively, have been eliminated. The resulting line densities are remarkably similar,  $\sim 4$  stars  $\text{pc}^{-1}$ ; only the L1495 group(s) exhibit much higher density. This line density implies an average distance to the nearest (stellar) neighbor of about 0.25 pc; this is similar to the estimated  $\sim 0.3$  pc for the median nearest-neighbor distance for all of Taurus found by Gomez et al. (1993), and is consistent with the break seen in the MSDC in Figure 6.

Masses are not available for all of the individual objects (for example, the Class I sources), and in any event mass determinations are subject to uncertainties in evolutionary tracks and binary/multiple companion masses. For the purpose of a rough comparison, it suffices to estimate the average system mass as about  $1M_\odot$ , a number arrived at by adopting the typical Taurus stellar mass of  $\sim 0.7M_\odot$  and recognizing that most objects in Taurus are members of multiple systems (Simon et al. 1995). The stellar bands in Taurus thus have a typical line density of roughly  $4M_\odot \text{ pc}^{-1}$ , approximately 1/4 of the the critical line density of the equilibrium isothermal filament at 10 K.

The stars in the groups constitute less mass than the associated gas. To estimate this, I turn to the  $\text{C}^{18}\text{O}$  survey of Taurus by Onishi et al. (1996, 1998). Adding up the masses of  $\text{C}^{18}\text{O}$  cores

identified in the B18 cloud (corresponding to the main region of Group 3) results in a total of  $126M_{\odot}$  spanning about 3.6 pc, or about  $35M_{\odot}\text{pc}^{-1}$ . As a check, a similar density  $\sim 30M_{\odot}\text{pc}^{-1}$  is found for the B213 filament (in Group 1). These values are approximately twice the critical density for the equilibrium isothermal filament at 10 K. (Note that Onishi et al. [1996] estimate a possible uncertainty of a factor of two in conversion from the  $\text{C}^{18}\text{O}$  measurements to total molecular hydrogen density.)

The difference between the average line densities of the stellar groups, which (outside of L1495) are about 1/4 of the critical value for a static isothermal cylinder, and that of the dense gas at about twice the critical value, indicates the limited efficiency of star formation at the present epoch. As star formation is clearly still continuing, given the large proportion of Class I sources in the groups, the stellar density may increase from the present value. If one adopts the estimate that the average age of the Taurus stars is  $\sim 2$  Myr (Palla & Stahler 2000), and that molecular clouds in the solar neighborhood disperse after a timescale of order 4 Myr or less (HBB), it is possible that Taurus is only about halfway through forming stars; in this case the ultimate stellar density in the groups might approach half the critical value, an efficiency of conversion of  $^{18}\text{CO}$  dense filamentary gas to stars of order 25%.

The average column density of the starless cores, as estimated by Onishi et al. (1998), is  $\sim 5 \times 10^{21}\text{cm}^{-2}$ , or  $A_V \sim 5$ . Inserting this value into equations (4), (5), and (8) yields  $\lambda_c \sim 0.3\text{pc}$ ,  $M_c \sim 5M_{\odot}$ , and  $\tau \sim 0.7$  Myr, all assuming hydrostatic equilibrium at 10 K. These size scales, masses, and lifetimes are comparable to the average properties estimated for  $\text{NH}_3$  or optical cores in Taurus (Jijina, Myers, & Adams 1999; Lee & Myers 1999).

This picture is consistent with the structure of the MSDC. Although Larson (1995) interpreted the break at  $\sim 0.02$  degree  $\sim 0.05$  pc as the Jeans length in Taurus, it seems more reasonable to interpret the break in the MSDC at 0.25 pc scale as the true average Jeans length. This is roughly consistent with the results of Blitz & Williams (1997), who found a characteristic length scale in  $^{13}\text{CO}$  emission in Taurus of order 0.25-0.5 pc, and similarly identified this with the Jeans length. It is possible that this length corresponds to the width of a filament, but this is closely related to the Jeans length as discussed above, and it is not clear how to distinguish these possibilities from the MSDC. In any event, because the protostellar clouds are not generally rotationally supported, collapse to a smaller structure will likely result in fragmentation into binaries or multiple systems with separations smaller than the original cloud Jeans length. This provides an explanation of the two breaks in the MSDC, one at the scale  $\log\theta \sim -1.7$  or  $r \sim 0.05$  pc marking the appearance of binary systems, and the other at 0.25 pc corresponding to the Jeans length.<sup>2</sup> Implicit in this discussion is the idea that the stars have not dispersed far from their birthsites, as suggested by the narrow distribution of Group 3.

---

<sup>2</sup>It is worth noting that Figure 1b of Simon (1997) suggests a similar break in the MSDC for Ophiuchus, but at a slightly smaller scale than in Taurus. This might indicate a smaller Jeans length in this higher-density region (but see Bate, Clarke, & McCaughrean 1998 for a discussion of some limitations of MSDC analyses).

One problem in comparing the observations with a static model is that the average velocity dispersion seen in the C<sup>18</sup>O cores ( $\sim 0.4 \text{ km s}^{-1}$  for starless regions) is considerably larger than the sound speed at 10 K,  $\sim 0.19 \text{ km s}^{-1}$  (although in the densest regions the velocity dispersion in the gas approaches the thermal value much more closely; Rydbeck et al. 1977; Myers, Linke, & Benson 1983; Barranco & Goodman 1999). Thus, the equilibrium cylinder may be used only as a guide to the true physical situation. However, the simulation of Nakajima & Hanawa (1996) of filament formation from a static sheet suggests that a relatively quiescent and static filament might be present for some reasonable period of time; in their model, supersonically-moving material which passes through a shock before accreting into the (relatively static) filament.

Onishi et al. (1998), who also proposed that gravitational fragmentation is operating in the C<sup>18</sup>O filaments, suggested that the line width should be interpreted in terms of an additional turbulent pressure support. If this were the case, changing the effective sound speed upward by a factor of two would increase the characteristic length scale to a value of order 1 pc, and the characteristic mass would be closer to  $30M_{\odot}$ . The situation might be even more complicated if a non-standard equation of state were used in which turbulent pressure increases with decreasing density (e.g., McLaughlin & Pudritz 1997). However, the observed velocity width may not represent simply pressure *support* but more complex motions (Ballesteros-Paredes, Vazquez-Semadeni, & Scalo 1999). If the average line density in the filaments really does exceed the critical value, the filaments could be collapsing radially, which might explain part of the observed velocity dispersion. Alternatively, one might be detecting the supersonic motions of material accreting onto (relatively static) filaments, as in the calculations of Nakajima & Hanawa (1996).

Another problem is the efficiency of star formation. It appears that only a fraction  $\sim 25\%$  of dense filament gas will become stars. Léorat, Passot, & Poquet (2000) and Klessen, Heitsch, & Mac Low (2000) showed that small scale driving is needed to prevent gravitational collapse. Outflows or other protostellar energy input on small scales from local sources, i.e. objects located within the filament, may be required to disperse filamentary gas and limit star formation (e.g., Adams & Fatuzzo 1996; Matzner & McKee 1999, 2000).

### 3.3. Protostellar core structure

This picture of gravitational fragmentation suggests that the fragmenting cores might be elongated (e.g., Schneider & Elmegreen 1979). The static model suggests aspect ratios of 2-3, as discussed above, comparable to the average aspect ratio for optical cores of 2.4 found by Lee & Myers (1999). Moreover, the cores show a tendency to be elongated along the filaments (e.g., Myers et al. 1991), as would be predicted by the static model. Figure 7 shows the spatial distribution and position angles of all elongated optical cores studied by Lee & Myers (1999). The cores tend to be elongated along the filamentary structure (Myers et al. 1991). The alignment is particularly strong in the group 3/B18/L1506 region; only 2 of the 13 cores have orientations deviating by more than about 30 degrees from the overall orientation of the filament. Note that Myers et al. (1991) showed

that many tracers -  $\text{NH}_3$ , extinction, etc. - show similar elongations on differing scales, and so the choice of optical core properties does not bias the results. It is also worth noting that Tachihara et al. (2000) found a similar trend for cores to be aligned with filaments in Ophiuchus.

Again, one must emphasize that static models are not necessarily applicable to the dynamic conditions in Taurus. However, the numerical simulations of Klessen & Burkert (2000) found that the gravitationally-unstable clumps were often elongated as part of a larger filamentary structure, suggesting that the qualitative results of the static stability analysis are relevant.

Some cores are aligned at large angles to the overall filamentary structure. However, in several cases these objects lie near more complex filamentary structure seen in  $^{13}\text{CO}$  (for example, the two cores near  $l=172$ ,  $b=-15.5$  are situated along a filamentary section which runs nearly perpendicular to the overall filamentary structure, as shown in Figure 3). The more complex structure seen in the  $^{13}\text{CO}$  map suggests that small-scale structure can play a non-negligible role in driving star formation. Along these lines, it is worth noting that the filamentary structure near the L1495 “double group” is quite complicated (cf. Figure 3), leading to the speculation that intersecting smaller-scale flows have led to building up a larger mass concentration which can then fragment into groups that are denser than the other filaments (cf. Table 2), a feature observed in the simulations of Klessen & Burkert (2000, 2001) and Klessen (2001).

Models of collapsing clouds indicate that close binary or multiple star formation is best achieved by clouds which are not highly centrally concentrated initially, and upon which some non-axisymmetric perturbation is imposed (Boss 1995, and references therein; Boss 1997; Bodenheimer et al. 2000). In this regard the collapse of an elongated cylinder might be nearly ideal for producing binaries (e.g., Boss 1993), which Taurus seems to do at a rate exceeding that of the field (Simon et al. 1995, and references therein).

In a recent paper Jones & Basu (2002; see also Jones, Basu, & Dubinski 2001) suggest that cores are in general triaxial, closer to prolate on large scales but more nearly oblate on small scales.<sup>3</sup> It is difficult to reconcile the picture of oblate cores with the filamentary organization of Taurus cores and their clear systematic orientation along the filaments, especially in group 3. Fragmentation out of a filament could produce oblate objects if contraction occurs along the filament; but then the long axes of the cores would be aligned perpendicular to the filament, not parallel as observed. In this context, Curry (2002) has performed an additional analysis of cores shapes and concluded that most are quasi-prolate, assuming random orientation of inclinations, and has also pointed out the likelihood of fragmenting cores out of filaments.

Alternatively, one might suppose that the Taurus filaments are more elongated along the line of sight than their minor axes projected upon the sky would indicate; in this way fragmentation into long pieces along the filament could be consistent with quasi-oblate objects. However, this would require that the sheets be viewed nearly edge-on to appear filamentary. A test of this idea would be

---

<sup>3</sup>The opposite conclusion was erroneously reported in the discussion in HBB.

to study core orientations relative to the larger-scale filamentary structure in other regions. If cores are systematically oriented closely along their natal filaments in most or all regions, it is unlikely that this can be attributed to projection effects, and would favor the quasi-prolate configuration.

It is also important to consider the evolution of a collapsing flattened structure. Consider for example the calculations performed by Hartmann et al. (1994) for the isothermal self-gravitating sheet. In the early stages of gravitational collapse, a central condensation initially forms which is much rounder than the initial configuration - this is a natural product of gravity operating on a scale of order the sheet scale height or smaller. This structure persists until material in the shortest dimension has been able to fall in. In other words, the cloud structure is not that of a uniform (quasi-) ellipsoid on all scales. This may be consistent with the finding of Jones & Basu (2002), who suggest that protostellar clouds are more prolate on large scales even if more oblate on small scales. A strong central density concentration which is more nearly spherical does not mean that the parent core was not highly elongated, nor that subsequent infall will be spherical. Observations with higher spatial resolution, spanning a wider range of densities, would be helpful in sorting among these possibilities.

### 3.4. Dynamic star formation

If protostellar cloud cores are generally (roughly) prolate, at least on larger scales, this poses problems for hydrostatic equilibrium models of cores supported primarily by magnetic fields. Curry & Stahler (2001) have developed models of quasi-static cores which are prolate; however, in these models the magnetic field is oriented along the major axis of the cloud. As noted in the previous section, the large-scale magnetic field in Taurus is more nearly perpendicular to the filaments and thus to the core elongations. While there are no direct measurements of field directions in the filaments, it is more plausible to suppose that the field remains roughly perpendicular to the core major axes than otherwise. The model of Fiege & Pudritz (2000), in which the filaments are constrained by fields with a modest helical component, cannot be ruled out in the absence of more detailed magnetic field measurements, but the maintenance of such helical components seems to require special conditions, e.g., fixing the ends of the helical magnetic field lines to maintain the twist. Curry (2000) has identified prolate equilibria in cylindrical geometry without magnetic fields; however, it is not clear that such solutions are relevant, given the observed high line densities and supersonic turbulence observed in the Taurus filaments.

It seems more likely that the cores are not in hydrostatic equilibrium (Fleck 1992), which would not require special conditions, though some regions may be relatively quiescent or quasi-static. Because the core lifetimes, of order a few  $\times 10^5$  yr (Lee & Myers 1999), are consistent with the linear growth times for gravitational collapse (§3.2), there is no need for exact hydrostatic equilibrium. It should be emphasized that if cores are gravitationally fragmenting from (low velocity-dispersion) filaments, the very act of their formation implies contraction on their largest scales, with subsonic motions during the linear growth regime, consistent with the large-scale, slow infall inferred by

Tafalla et al. (1998) and Lee, Myers, & Tafalla (2001).

In a dynamic picture, all that is required is that shock dissipation of turbulent motions produces subsonic flows, in which cores can gravitationally fragment (Padoan & Nordlund 1999; Klessen & Burkert 2000, 2001). Although cores are unlikely to be in hydrostatic equilibrium, they may start their existence as subsonically-evolving objects in the post-shock gas; for this reason static models of cores still can be used a guide to the more complex physics of real cores.

These considerations suggest the following, highly schematic, picture of low-mass star formation in Taurus (Figure 8). Large-scale flows might form either filaments or more likely sheet-like structures (Figure 8a), which becomes molecular when the accumulated surface density is large enough that  $A_V \gtrsim 1$ ; at this point, self-gravity of the layer becomes important (HBB). An initially sheet-like configuration might collapse laterally to form filaments, either due to turbulent instabilities or gravitational contraction, (Figure 8b, middle figure, side view). The turbulence driven by the flows has a large-scale component, possibly associated with and/or channeled by the large-scale magnetic field; this results in contraction into extended bands or low density filaments. The densest regions of these contracting filaments, where secondary shocks have dissipated more of the turbulent motions, gravitationally fragment into elongated structures which correspond to protostellar cloud cores (Figure 8b, bottom figure, top view).

This model is clearly highly schematic; Figure 3 shows that individual dense filaments can be much more complex in structure than outlined here. Furthermore, even at a schematic level this might not necessarily apply to all star formation in Taurus; roughly 60% of the total population do not fall into groups 1-4, and the geometry of the more “clustered” groups (L1495, L1551) is different. On the other hand, it must be recognized that dispersal of gas and stars, which has clearly gone on in Taurus to some extent, will tend to erase any initial structure. Even if the gaseous structure is more complicated in general than long straight filaments (e.g., Figure 3), the qualitative aspects of sheet formation by flows, flow-driven or gravitational contraction into filaments due to anisotropic turbulent and magnetic pressures, followed by protostellar core fragmentation from filaments may still be applicable.

#### 4. Conclusions

The spatial distribution of young stars in Taurus is remarkably filamentary and well-organized. The large-scale coherence of the spatial distribution suggests that small-scale turbulence is not dominating the cloud structure, consistent with driving by external flows which could have formed the cloud. The spatial distribution of young stars is consistent with a roughly uniform distribution along bands and filaments, with a spacing comparable to the local Jeans length. The efficiency of star formation in filaments is much higher than elsewhere; the higher frequency of protostars and accreting T Tauri stars indicates that the population in these filaments is relatively young. The protostellar cores from which the stars formed are often elongated along the filaments in which they

reside, consistent with formation by gravitational fragmentation. Fragmentation of filaments naturally produces elongated, roughly prolate cloud cores whose structure is well-suited to producing binaries after collapse. Numerical simulations of turbulent clouds with higher spatial resolution, and turbulent driving on large scales, are urgently needed to compare with the observations of this nearby region which constitutes the main example of “quiescent” star formation.

The fragmentation of filaments into stars in Taurus has an echo on larger scales in regions of high mass and clustered star formation, a topic addressed in the second paper in this series.

The discussion of this paper was strongly influenced by my collaboration with Javier Ballesteros, especially the many discussions we have had concerning turbulent support. The paper also benefited greatly from the suggestions, comments, and encouragement of Phil Myers, who also suggested the importance of the roughly periodic banded/filamentary structure of Taurus, and its implications in terms of fragmentation from a sheet-like structure. This work was supported in part by NASA grant NAG5-9670.

## REFERENCES

- Adams, F. C. & Fatuzzo, M. 1996, *ApJ*, 464, 256
- André, P., Motte, F., & Bacmann, A. 1999, *ApJ*, 513, L57
- Ballesteros-Paredes, J., Hartmann, L., & Vazquez-Semadeni, E. 1999, *ApJ*, 527, 285 (BHV)
- Ballesteros-Paredes, J., Vazquez-Semadeni, E., & Scalo, J. 1999, *ApJ*, 515, 286
- Barranco, J. A. & Goodman, A. A. 1998, *ApJ*, 504, 207
- Bate, M. R., Clarke, C. J., & McCaughrean, M. J. 1998, *MNRAS*, 297, 1163
- Blitz, L. & Williams, J. P. 1997, *ApJ*, 488, L145.
- Boss, A. P. 1993, *ApJ*, 410, 157
- Boss, A. P. 1995, *Rev. Mex. Astr. Astrof., Conference Series*, 1, 165
- Boss, A. P. 1997, *ApJ*, 483, 309
- Bodenheimer, P., Burkert, A., Klein, R. I., & Boss, A. P. 2000, in *Protostars and Planets IV*, eds. Mannings, V., Boss, A. P., & Russell, S. S., University of Arizona Press, Tucson, 675
- Briceño, C., Calvet, N., Kenyon, S., & Hartmann, L. 1999, *AJ*, 118, 1354
- Briceño, C., Hartmann, L. W., Stauffer, J. R., Gagne, M., Stern, R. A., & Caillault, J. 1997, *AJ*, 113, 740
- Briceño, C., Hartmann, L., Stauffer, J., & Martín, E. 1998, *AJ*, 115, 2074
- Burkert, A., & Mac Low, M.-M. 2002, submitted to *ApJ*
- Chandrasekhar, S. & Fermi, E. 1953, *ApJ*, 118, 116



- Chen, H., Myers, P. C., Ladd, E. F., & Wood, D. O. S. 1995, *ApJ*, 445, 377
- Curry, C.L. 2000, *ApJ*, 541, 831
- Curry, C.L. 2002, *ApJ*, in press (astro-ph/0206311)
- Curry, C. L. & Stahler, S. W. 2001, *ApJ*, 555, 160
- Elmegreen, B. G. 1997, *ApJ*, 486, 944
- Elmegreen, B. G. 2000, *ApJ*, 530, 277
- Falgarone, E., Panis, J.-F., Heithausen, A., Perault, M., Stutzki, J., Puget, J.-L., & Bensch, F. 1998, *A&A*, 331, 669
- Fiege, J. D. & Pudritz, R. E. 2000, *ApJ*, 534, 291
- Fleck, R.C. Jr. 1992, *ApJ*, 401, 146
- Gomez, M., Jones, B.F., Hartmann, L., Kenyon, S.J., Stauffer, J.R., Hewett, R. & Reid, I.N. 1992, *AJ*, 104, 762
- Gomez, M., Hartmann, L., Kenyon, S. J., & Hewett, R. 1993, *AJ*, 105, 1927
- Hartmann, L. 2001, *AJ*, 121, 1030
- Hartmann, L., Ballesteros-Paredes, J., & Bergin, E. 2001, *ApJ*, 562, 852
- Hartmann, L., Boss, A., Calvet, N., & Whitney, B. 1994, *ApJ*, 430, L49
- Heitsch, F., Mac Low, M., & Klessen, R. S. 2001, *ApJ*, 547, 280
- Heyer, M. H., Vrba, F. J., Snell, R. L., Schloerb, F. P., Strom, S. E., Goldsmith, P. F., & Strom, K. M. 1987, *ApJ*, 321, 855
- Jijina, J., Myers, P. C., & Adams, F. C. 1999, *ApJS*, 125, 161
- Jones, C.E., & Basu, S. 2002, *ApJ*, 569, in press
- Jones, C. E., Basu, S., & Dubinski, J. 2001, *ApJ*, 551, 387
- Jones, B. F. & Herbig, G. H. 1979, *AJ*, 84, 1872
- Kenyon, S. J., Dobrzycka, D., & Hartmann, L. 1994, *AJ*, 108, 1872
- Kenyon, S. J. & Hartmann, L. 1995, *ApJS*, 101, 117
- Klein, R. I. & Woods, D. T. 1998, *ApJ*, 497, 777.
- Klessen, R.S. 2001, *ApJ*, 556, 837
- Klessen, R. S. & Burkert, A. 2000, *ApJS*, 128, 287
- Klessen, R. S. & Burkert, A. 2001, *ApJ*, 549, 386
- Klessen, R.S., Heitsch, F. & MacLow, M. 2000, *ApJ*, 535, 887
- LaRosa, T.N., Shore, S.N., & Magnani, L. 1999, *ApJ*, 512, 761
- Larson, R.B. 1981, *MNRAS*, 194, 809

- Larson, R.B. 1985, MNRAS, 214, 379
- Larson, R.B. 1995, MNRAS, 272, 213
- Lee, C.W. & Myers, P.C. 1999, ApJS, 123, 233
- Lee, C. W., Myers, P. C., & Tafalla, M. 2001, ApJS, 136, 703
- Leorat, J., Passot, T. & Pouquet, A. 1990, MNRAS, 243, 293
- Mac Low, M.-M. 1999, ApJ, 524, 169
- Mac Low, M.-M., Klessen, R. S., Burkert, A., & Smith, M. D. 1998, Phys. Rev. Lett., 80, 275
- Martín, E. L. & Magazzù, A. 1999, A&A, 342, 173
- Matzner, C. D. & McKee, C. F. 2000, ApJ, 545, 364
- Matzner, C. D. & McKee, C. F. 1999, ApJ, 526, L109
- McLaughlin, D. E. & Pudritz, R. E. 1997, ApJ, 476, 750
- Megeath, T., Dame, T., & Thaddeus, P. 2002, in preparation
- Miyama, S.M., Narita, S., & Hayashi, C. 1987a, Prog. Theoretical Physics, 78, 1051
- Miyama, S.M., Narita, S., & Hayashi, C. 1987b, Prog. Theoretical Physics, 78, 1273
- Mizuno, A., Onishi, T., Yonekura, Y., Nagahama, T., Ogawa, H., & Fukui, Y. 1995, ApJ, 445, L161
- Moneti, A., Pipher, J. L., Helfer, H. L., McMillan, R. S., & Perry, M. L. 1984, ApJ, 282, 508
- Myers, P. C., Fuller, G. A., Goodman, A. A., & Benson, P. J. 1991, ApJ, 376, 561
- Myers, P. C., Linke, R. A., & Benson, P. J. 1983, ApJ, 264, 517.
- Nakajima, Y. & Hanawa, T. 1996, ApJ, 467, 321
- Neuhäuser, R., Sterzik, M. F., Schmitt, J. H. M. M., Wichmann, R., & Krautter, J. 1995, A&A, 295, L5
- Oganessian, R. S. 1960a, Soviet Astronomy, 4, 434
- Oganessian, R. S. 1960b, Soviet Astronomy, 4, 634
- Onishi, T., Mizuno, A., Kawamura, A., Ogawa, H., & Fukui, Y. 1996, ApJ, 465, 815
- Onishi, T., Mizuno, A., Kawamura, A., Ogawa, H., & Fukui, Y. 1998, ApJ, 502, 296
- Ostriker, E. C., Stone, J. M., & Gammie, C. F. 2001, ApJ, 546, 980
- Ostriker, J. 1964, ApJ, 140, 1056
- Padoan, P. & Nordlund, Åke 1999, ApJ, 526, 279
- Palla, F. & Stahler, S. W. 2000, ApJ, 540, 255
- Pringle, J. E., Allen, R. J., & Lubow, S. H. 2001, MNRAS, 327, 663

- Rydbeck, O. E. H., Sume, A., Hjalmarson, A., Ellder, J., Ronnang, B. O., & Kollberg, E. 1977, ApJ, 215, L35.
- Sakamoto, S. 2002, ApJ, 565, 1050
- Scalo, J. 1990, in Physical processes in fragmentation and star formation (Dordrecht: Kluwer), 151
- Schneider, S. & Elmegreen, B. G. 1979, ApJS, 41, 87
- Shu, F.H., Adams, F.C., & Lizano, S. 1987, ARAA, 25, 23
- Simon, M. 1997, ApJ, 482, L81
- Simon, M., Ghez, A.M., Leinert, Ch., Cassar, L., Chen, W.P., Howell, R.R., Jameson, R.F., Matthews, K., Neugebauer, G., Richichi, A. 1995, ApJ, 443, 625
- Stone, J. M., Ostriker, E. C., & Gammie, C. F. 1998, ApJ, 508, L99
- Tachihara, K., Mizuno, A., & Fukui, Y. 2000, ApJ, 528, 817
- Tafalla, M., Mardones, D., Myers, P. C., Caselli, P., Bachiller, R., & Benson, P. J. 1998, ApJ, 504, 900
- Walter, F. M., Brown, A., Mathieu, R. D., Myers, P. C., & Vrba, F. J. 1988, AJ, 96, 297
- Wichmann, R. et al. 1996, A&A, 312, 439
- Wichmann, R., Torres, G., Melo, C.H.F., Frink, S., Allain, S., Bouvier, J., Krautter, J., Covino, E., & Neuhäuser, R. 2000, A&A, 359, 181

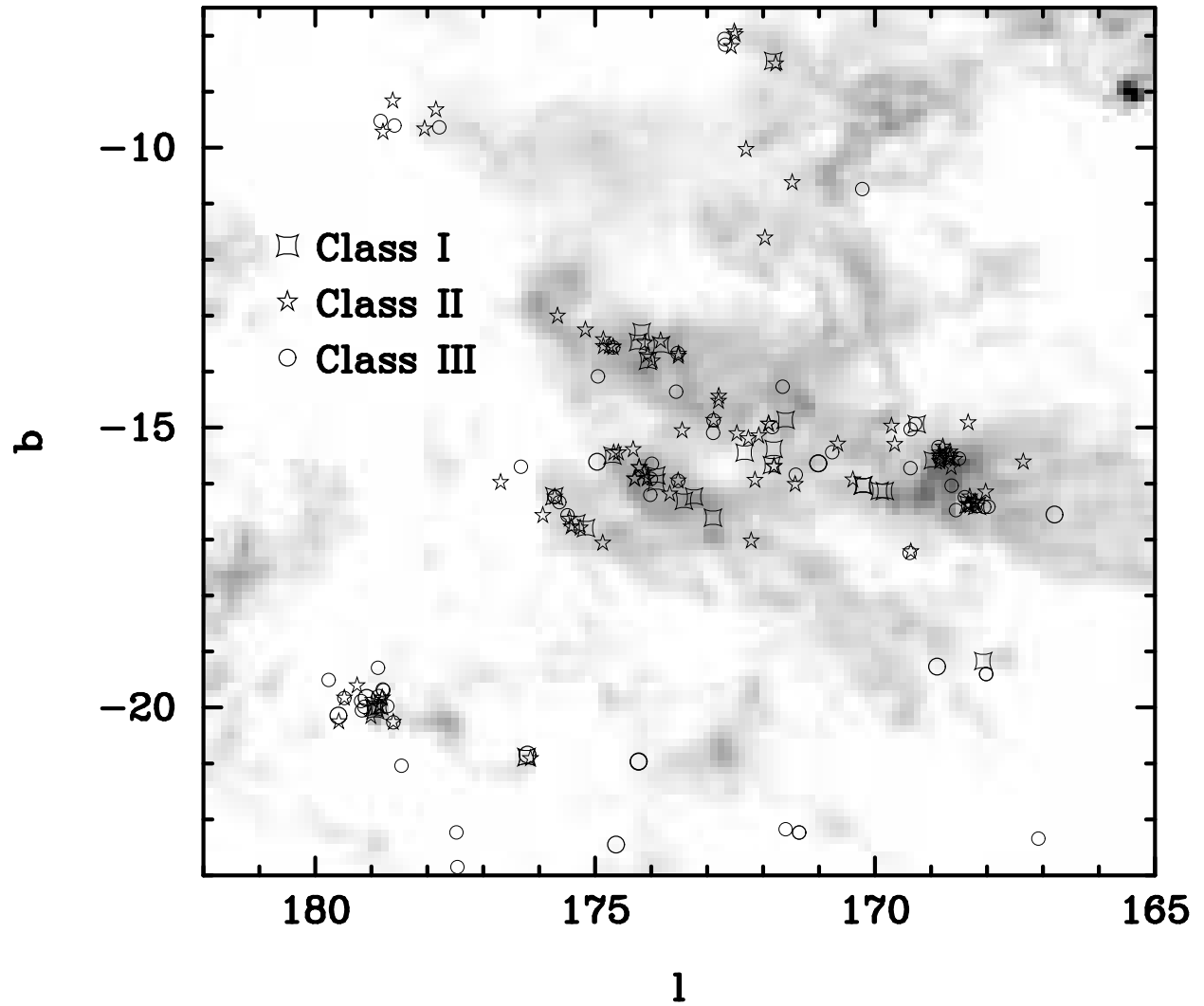


Fig. 1.— Young stellar objects in the Taurus region, labelled by their spectral energy distribution class, superimposed upon the  $^{12}\text{CO}$  map of Megeath, Dame, & Thaddeus (2002) (see text)

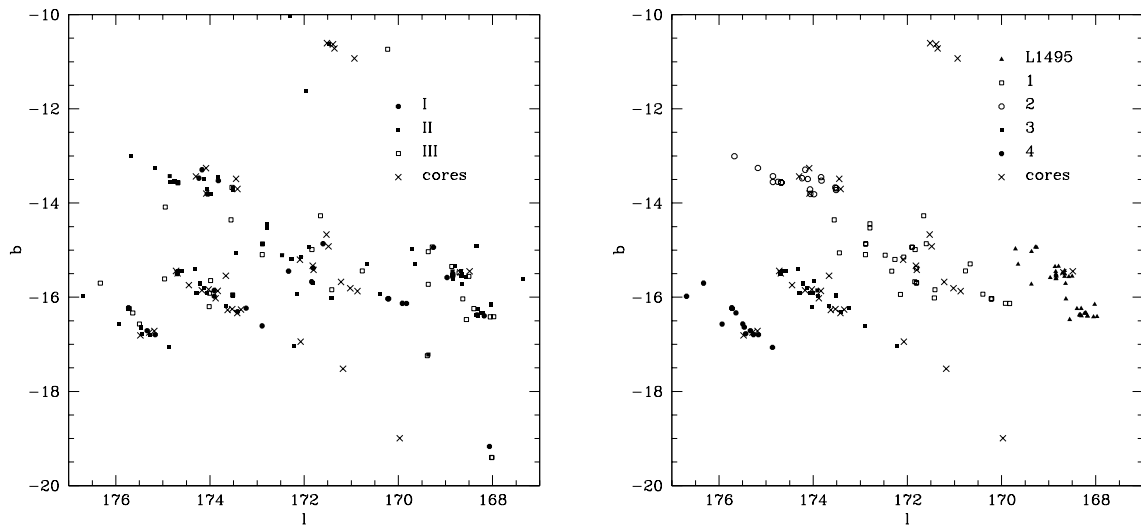


Fig. 2.— a) Spatial distribution of young stars, labelled by their spectral energy distribution class, and optically-selected cores in the central region of Figure 1; b) Subset of stars in a) associated with groups, as labeled in the legend (see text; also Table 1)

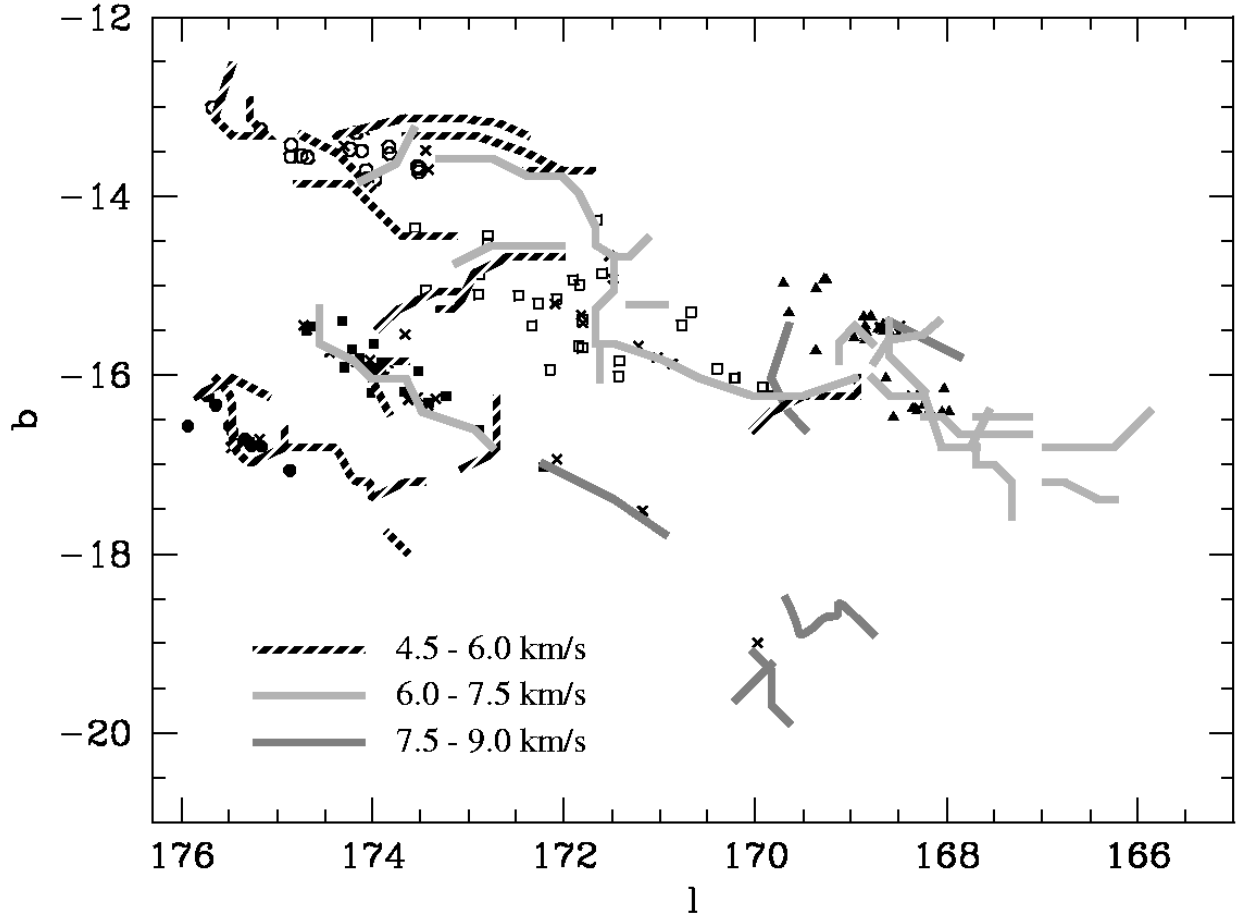


Fig. 3.— Approximate position of  $^{13}\text{CO}$  filaments in the central region of Taurus found by Mizuno et al. (1995), superimposed upon the groups of Figure 2b. The CO filaments are sorted into the same LSR velocity range as shown by Mizuno et al. .

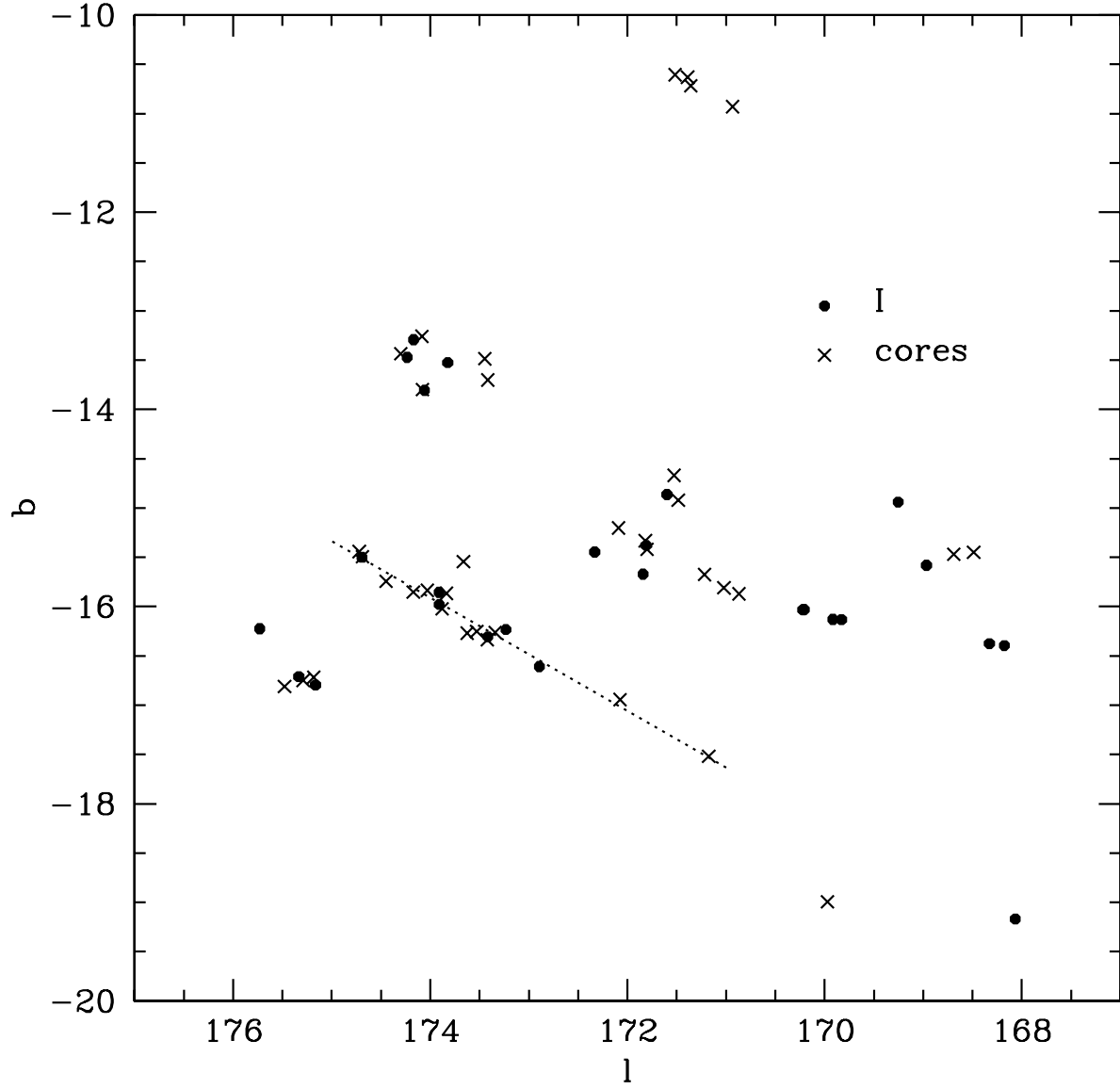


Fig. 4.— Spatial distribution of Class I objects and optical cores from the survey of Lee & Myers (1999). The dotted line is a least squares linear fit to the objects in the region of group 3 (see text)

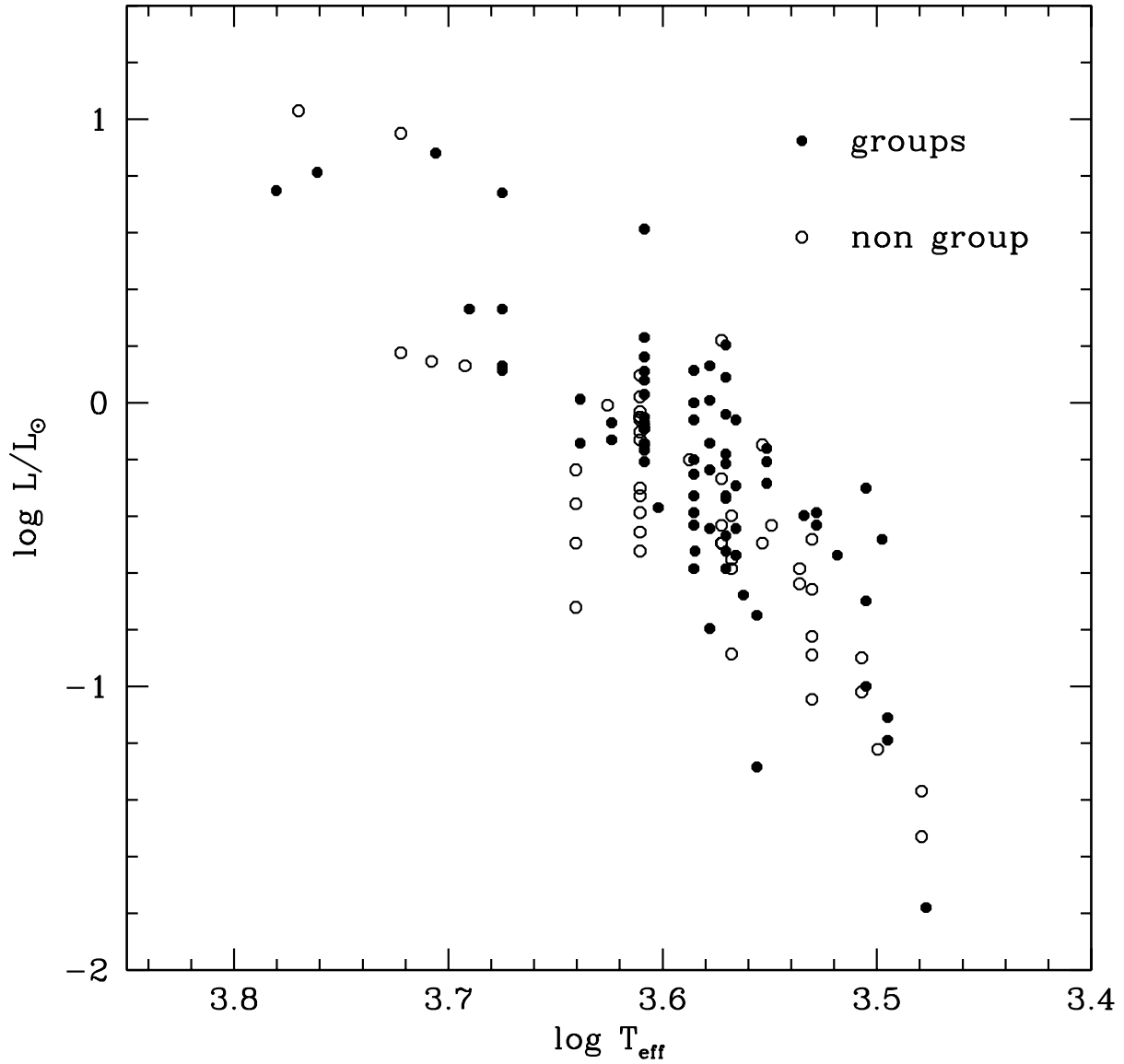


Fig. 5.— HR diagram for stars with available stellar luminosities and effective temperatures (see text), sorted between members of the groups and others. The group stars appear to be somewhat younger than the non-group objects, though the result is marginal due to possible systematic errors (see text)



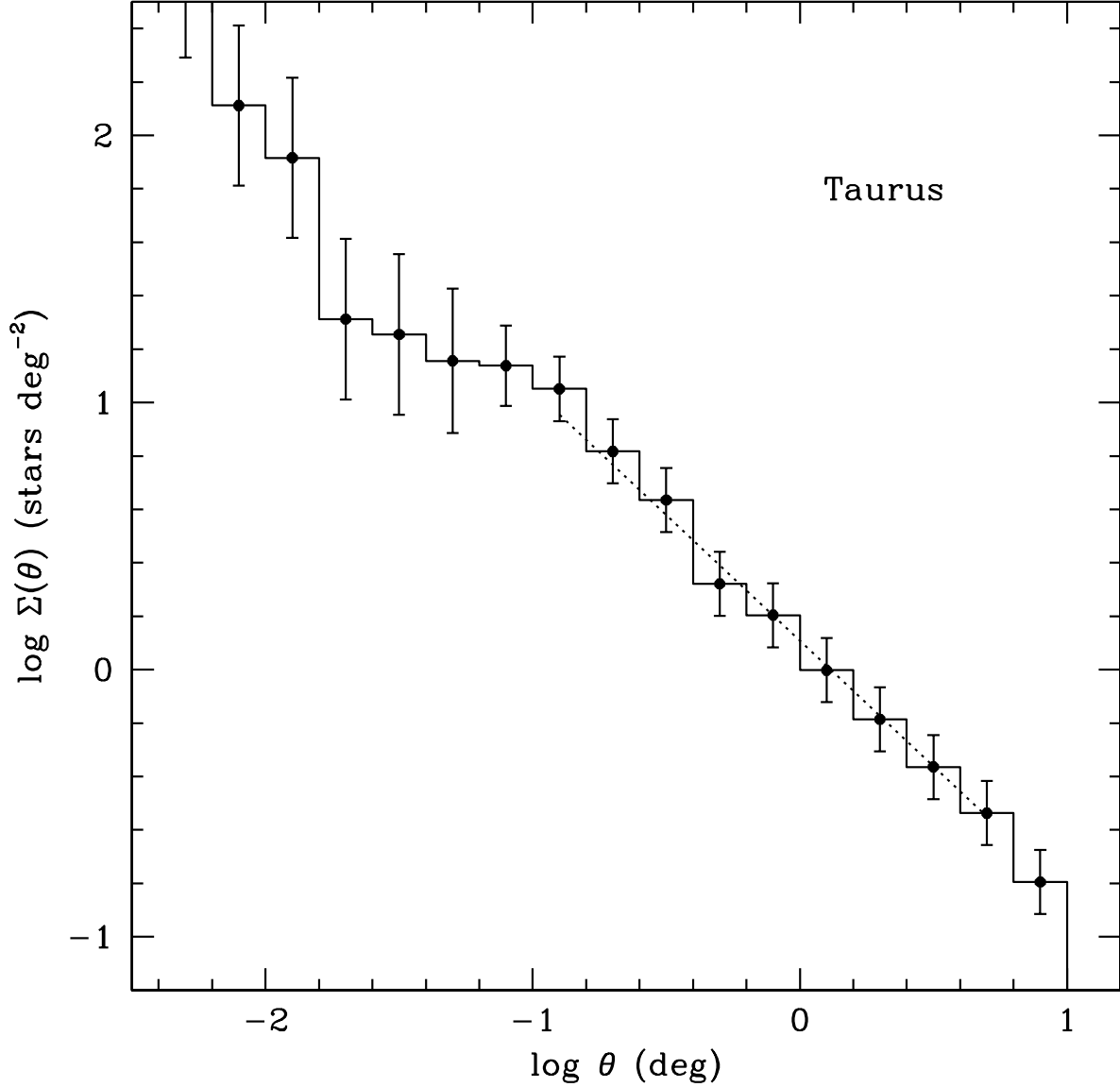


Fig. 6.— The mean surface density of companions (MSDC),  $\Sigma(\theta)$ , as a function of angular separation  $\theta$  (degrees). The dotted line is a least-squares linear fit with slope  $-0.98$  to the bins between  $-0.9 \leq \log \theta \leq 0.7$ . At small separations the MSDC rises rapidly due to binary and multiple companions. The break in slope at  $\log \theta \sim -1$  corresponds to a spatial separation of about  $0.24$  pc at the distance of Taurus.

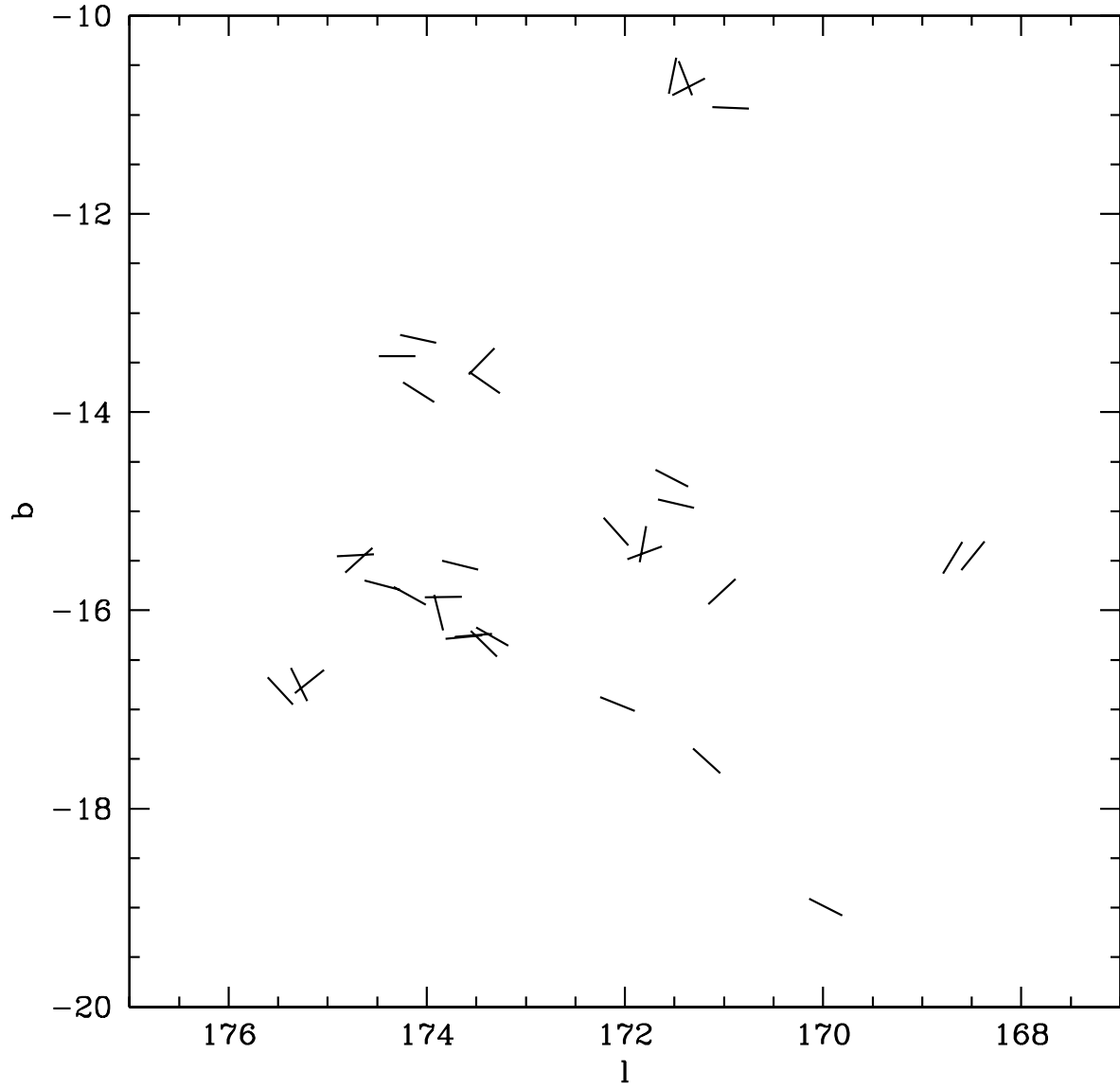


Fig. 7.— Spatial distribution of optical cores from Lee & Myers (1999), with the orientation of the line indicating the position angle of the core major axis.

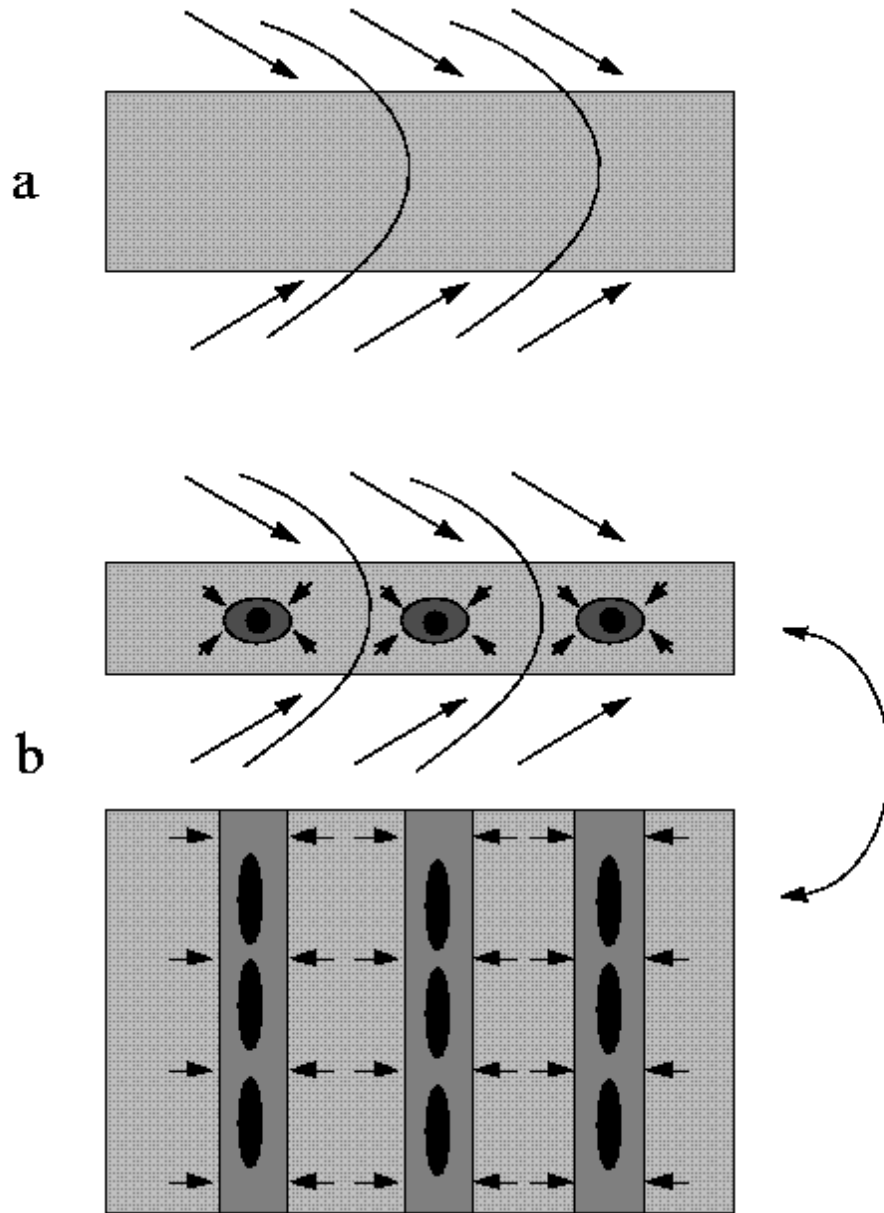


Fig. 8.— Suggested outline of star formation in Taurus filaments. Converging large-scale flows in the interstellar medium form a sheet-like structure (a). Magnetic fields may help channel the flow. When sufficient column density is amassed, sheet is subject to gravitational fragmentation into filaments (b) (e.g., Schneider & Elmegreen 1979; Miyama et al. 1987a,b; Nakajima & Hanawa 1996), possibly aided by anisotropic (large-scale) turbulence and/or magnetic field channelling. The collapsing filaments develop dense cores (top view, bottom part of (b)) which then fragment into protostellar cores (see text).

Table 1. Taurus Groups

l	b	RA(1950)	Dec(1950)	Name	Class
Group 1					
169.8285	-16.1320	04:16:38.30	27:06:23.0	04166+2706	I
169.9167	-16.1288	04:16:54.60	27:02:49.0	04169+2702	I
170.2079	-16.0303	04:18:05.50	26:54:37.0	04181+2655	I
170.2185	-16.0327	04:18:06.90	26:54:04.0	04181+2654A	I
170.2185	-16.0327	04:18:06.90	26:54:04.0	04181+2654B	I
171.8103	-15.3798	04:24:53.70	26:12:41.0	04248+2612	I
172.3320	-15.4465	04:26:09.80	25:47:30.0	04361+2547	I
171.5982	-14.8631	04:26:00.30	26:42:31.0	04260+2642	I
170.3973	-15.9353	04:18:57.60	26:50:30.5	FS Tau	II
170.6678	-15.2938	04:21:52.10	27:05:08.0	IP Tau	II
171.4271	-16.0164	04:21:41.30	26:03:30.0	04216+2603	II
171.8052	-15.6962	04:23:49.90	26:00:13.0	FV Tau	II
171.8080	-15.6946	04:23:50.70	26:00:09.7	FV Tau/c	II
171.8424	-15.6720	04:24:01.10	25:59:35.5	DG Tau	II
171.8990	-14.9386	04:26:37.10	26:26:28.9	DH Tau	II
171.9033	-14.9377	04:26:38.00	26:26:20.0	DI Tau	II
172.0771	-15.1492	04:26:25.55	26:10:22.6	FW Tau=CIDA4	II
172.1465	-15.9423	04:23:59.60	25:35:41.7	DF Tau	II
172.2647	-15.1990	04:26:47.70	26:00:16.0	IQ Tau	II
172.4695	-15.1082	04:27:40.80	25:54:59.0	DK Tau	II
172.7942	-14.4392	04:30:50.50	26:07:14.0	IT Tau=J 644	II
172.7966	-14.5294	04:30:32.70	26:03:34.5	IS Tau	II
172.8864	-14.8703	04:29:39.30	25:46:13.0	UZ Tau e	II
173.4457	-15.0568	04:30:36.00	25:14:24.0	DL Tau	II
171.8363	-14.9900	04:26:16.00	26:27:09.0	J 507	III
170.7675	-15.4414	04:21:40.30	26:54:54.0	J 4423	III
171.4156	-15.8420	04:22:13.80	26:11:02.0	J 4872	III
171.6520	-14.2686	04:28:09.10	27:03:54.0	JH 56	III
172.8864	-14.8703	04:29:39.30	25:46:13.0	UZ Tau w	III
172.8913	-15.0952	04:28:55.00	25:37:08.0	J 665	III

Table 1—Continued

l	b	RA(1950)	Dec(1950)	Name	Class
173.5555	-14.3572	04:33:15.40	25:36:55.0	LkCa 14	III
Group 2					
173.8235	-13.5257	04:36:49.30	25:57:16.0	04368+2557	I
174.0586	-13.8065	04:36:31.20	25:35:56.0	04365+2535	I
174.2349	-13.4732	04:38:08.50	25:40:53.0	04381+2540	I
173.5117	-13.6870	04:35:24.20	26:04:55.0	DO Tau	II
173.5146	-13.7251	04:35:16.91	26:03:18.6	GM Tau=CIDA5	II
173.8322	-13.4512	04:37:06.00	25:59:45.0	04370+2559	II
173.9804	-13.8124	04:36:16.98	25:39:11.5	GN Tau	II
174.0667	-13.7120	04:36:51.80	25:39:13.0	IC 2087 IR	II
174.1151	-13.4909	04:37:45.00	25:45:34.0	JH 223	II
174.1697	-13.2929	04:38:34.60	25:50:44.0	04385+2550	II
174.6803	-13.5606	04:39:04.20	25:17:32.8	V955 Tau	II
174.6803	-13.5645	04:39:03.40	25:17:23.7	CoKu LkH332G1	II
174.7475	-13.5498	04:39:17.45	25:14:56.1	CIDA-7	II
174.8543	-13.4296	04:39:59.60	25:14:43.0	GO Tau	II
174.8544	-13.5532	04:39:34.30	25:09:59.9	DP Tau	II
175.1741	-13.2561	04:41:27.50	25:06:53.0	04414+2506	II
175.6718	-13.0074	04:43:39.54	24:53:42.60	RXJ04467+2459	II
173.5306	-13.6696	04:35:30.90	26:04:45.2	HV Tau	III
174.6784	-13.5698	04:39:02.00	25:17:16.8	CoKu LkH332/G2	III
Group 3					
172.8944	-16.6094	04:23:54.50	24:36:54.0	04239+2436	I
173.2329	-16.2331	04:26:05.70	24:37:17.0	04264+2433	I
173.4157	-16.3056	04:26:21.90	24:26:30.0	GV Tau	I
174.6927	-15.5004	04:32:33.50	24:02:15.0	04325+2402	I
173.9105	-15.8558	04:29:13.60	24:22:42.9	Haro 6-13	I/II
173.9094	-15.9788	04:28:48.90	24:17:56.0	HK Tau	I/II
172.2120	-17.0264	04:20:37.20	24:49:20.0	FT Tau	II

Table 1—Continued

l	b	RA(1950)	Dec(1950)	Name	Class
173.5194	-15.9525	04:27:49.30	24:35:56.9	ZZ Tau IRS	II
173.6685	-16.1851	04:27:27.90	24:20:18.0	FX Tau	II
174.0690	-15.9106	04:29:28.90	24:13:38.6	FY Tau	II
174.0709	-15.9062	04:29:30.10	24:13:44.0	FZ Tau	II
174.1313	-15.8091	04:29:59.43	24:14:53.54	MHO-8	II
174.2137	-15.7127	04:30:32.30	24:15:03.0	GI Tau	II
174.2172	-15.7135	04:30:32.70	24:14:52.0	GK Tau	II
174.2939	-15.9146	04:30:05.20	24:03:39.0	V807 Tau	II
174.2974	-15.9196	04:30:04.80	24:03:18.0	GH Tau	II
174.3207	-15.3951	04:31:53.50	24:22:44.0	AA Tau	II
174.5856	-15.4517	04:32:25.70	24:08:52.0	DN Tau	II
174.6716	-15.4528	04:32:39.60	24:05:01.8	CoKu Tau/3	II
173.5194	-15.9525	04:27:49.30	24:35:56.9	ZZ Tau	III
173.9893	-15.6471	04:30:08.30	24:27:26.7	V830 Tau	III
174.0062	-15.9172	04:29:17.20	24:16:07.5	V928 Tau	III
174.0170	-16.2016	04:28:22.40	24:04:29.7	V927 Tau	III
Group 4					
175.1648	-16.7957	04:29:32.20	22:51:11.0	04295+2251	I
175.3343	-16.7109	04:30:16.40	22:47:04.0	04302+2247	I
175.7293	-16.2243	04:32:56.80	22:48:31.0	Haro 6-28	I
174.8657	-17.0661	04:27:50.20	22:53:40.0	04278+2253	II
175.2680	-16.7936	04:29:49.30	22:46:45.0	JH 112	II
175.4321	-16.7747	04:30:19.50	22:40:18.0	04303+2240	II
175.4641	-16.6360	04:30:52.20	22:44:16.7	CI Tau	II
175.7222	-16.2382	04:32:52.90	22:48:17.7	HP Tau	II
175.9349	-16.5703	04:32:20.80	22:26:06.6	HO Tau	II
176.6895	-15.9814	04:36:18.40	22:15:12.7	LkCa 15	II
175.4964	-16.5670	04:31:11.10	22:45:32.0	JH 108	III
175.6401	-16.3325	04:32:20.90	22:48:16.8	FF Tau	III
175.7222	-16.2382	04:32:52.90	22:48:17.7	HP Tau/G2	III
175.7222	-16.2382	04:32:52.90	22:48:17.7	HP Tau/G3	III

Table 1—Continued

l	b	RA(1950)	Dec(1950)	Name	Class
176.3280	-15.7005	04:36:17.40	22:42:02.0	VY Tau	III
L 1495					
168.1774	-16.3955	04:10:49.30	28:03:57.0	04108+2803 B	I
168.0247	-16.1523	04:11:08.60	28:20:26.9	FN Tau	II
168.1756	-16.4005	04:10:48.00	28:03:49.0	04108+2803 A	II
168.2101	-16.3310	04:11:07.80	28:05:18.8	FM Tau	II
168.2166	-16.3397	04:11:07.30	28:04:41.0	V773 Tau	II
168.2426	-16.3436	04:11:11.30	28:03:27.0	CW Tau	II
168.3044	-16.3975	04:11:12.09	27:58:38.6	CIDA-1	II
168.3096	-16.2403	04:11:43.60	28:05:01.6	FO Tau	II
168.3288	-16.3761	04:11:20.71	27:58:32.46	MHO-1	II
168.3289	-16.3757	04:11:20.80	27:58:33.0	04113+2758	II
168.3295	-16.3762	04:11:20.81	27:58:30.46	MHO-2	II
168.3500	-16.3743	04:11:24.92	27:57:44.73	MHO-3	II
168.5722	-15.5660	04:14:43.35	28:22:18.5	CIDA-3	II
168.6409	-15.7095	04:14:27.70	28:13:28.6	CY Tau	II
168.6559	-15.5033	04:15:10.93	28:21:25.53	v410a13	II
168.6626	-15.4350	04:15:25.60	28:23:59.0	04154+2823	II
168.8353	-15.5492	04:15:34.50	28:12:01.8	V892 Tau	II
168.8406	-15.5993	04:15:25.60	28:09:44.0	CZ Tau	II
168.7902	-15.3457	04:16:06.40	28:22:21.0	FQ Tau	II
168.8454	-15.6063	04:15:25.10	28:09:14.6	DD Tau	II
168.8490	-15.5064	04:15:45.40	28:13:14.0	CoKu Tau/1	II
168.8499	-15.4543	04:15:55.82	28:15:21.47	v410xr5a	II
168.9670	-15.5824	04:15:51.80	28:05:09.0	04158+2805	II
169.2547	-14.9396	04:18:50.90	28:19:35.0	RY Tau	II
169.6484	-15.3018	04:18:49.80	27:48:05.0	DE Tau	II
169.7051	-14.9734	04:20:05.10	27:59:08.0	04200+2759	II
168.6649	-15.5575	04:15:01.90	28:18:48.0	v410xr3	II
167.9731	-16.4132	04:10:08.46	28:11:35.2	LkCa 1	III
168.0482	-16.4167	04:10:21.54	28:08:21.5	Anon 1	III

Table 1—Continued

l	b	RA(1950)	Dec(1950)	Name	Class
168.3986	-16.2417	04:11:59.57	28:01:17.8	CIDA-2	III
168.5014	-15.5550	04:14:32.62	28:25:42.6	LkCa 5	III
168.5554	-16.4745	04:11:42.80	27:45:05.0	LkCa 3	III
168.6330	-16.0356	04:13:22.40	28:00:13.0	LkCa 4	III
168.7099	-15.4826	04:15:24.83	28:20:01.7	V410 Tau	III
168.8413	-15.5222	04:15:40.90	28:12:54.0	Hubble 4	III
168.8460	-15.5488	04:15:36.52	28:11:36.20	v410xr7	III
168.8670	-15.3480	04:16:19.90	28:19:02.6	V819 Tau	III
169.2815	-14.9352	04:18:56.60	28:18:37.7	LkCa 21	III
169.3654	-15.0320	04:18:52.50	28:11:06.6	HD 283572	III
169.3675	-15.7256	04:16:35.80	27:42:28.0	LkCa 7	III

Table 2. Density of Taurus groups

Group	N(YSO)	N(main) <sup>a</sup>	l(deg)	N /l(deg)	N /l(pc)
1	31	31	4.01	7.7	3.2
2	19	18	1.67	10.8	4.4
1+2	50	49	5.92	8.3	3.4
3	23	22	2.06	10.7	4.4
4	15	13	1.17	11.1	4.5
L1495	40	40	2.20	18.2	7.4

<sup>a</sup>Total number of stars considered, with outlying objects eliminated (see text): easternmost object in Group 2, westernmost object in Group 3, and the two easternmost members of Group 4 were eliminated.